

# Obtaining Ni Nanoparticles on 3Y-TZP Powder from Nickel Salts

Fátima Esteban-Betegón, Sonia Lopez-Esteban, Joaquín Requena, Carlos Pecharrmán, and José S. Moya<sup>\*\*†</sup>

Instituto de Ciencia de Materiales de Madrid, CSIC, 28049 Madrid, Spain

José C. Conesa

Instituto de Catálisis y Petroleoquímica, CSIC, 28049 Madrid, Spain

**Non-agglomerated and homogeneously dispersed nickel nanoparticles were obtained on the surface of zirconia particles from the solution of three different nickel salts (nitrate, chloride, and acetate) in ethanol. After a drying process, the powders were calcined and reduced. Transmission electron microscopy studies only showed a uniform distribution of Ni nanoparticles on the zirconia grain surfaces in the case of nickel obtained from nitrate salt. The analysis of the magnetic hysteresis loop of these particles has revealed the absence of Ni particles larger than 50 nm. Mechanisms to justify the different Ni particle sizes obtained from several salts have been proposed based on X-ray photoelectron and infrared spectroscopy. As a result, only in the case of a good zirconia/nickel nanostructure in the green samples and using nitrate salt dense (98% th.) nanocrystalline ceramic composites were obtained as a precursor.**

## I. Introduction

CERAMIC/METAL composite materials (cermets) have attracted significant attention because of a singular combination of properties (including mechanical, electrical, and magnetic) that makes them excellent candidates for the fabrication of multifunctional devices. Moreover, the fact that one of the phases is nanostructured substantially modifies the mechanical,<sup>1–3</sup> electrical,<sup>4</sup> magnetoresistive,<sup>5</sup> and magnetic properties.<sup>6–8</sup>

Different preparation processes of ceramic–metal nanocomposite powder can be found in the literature.<sup>9–12</sup> Thin-film deposition methods produce monodisperse nanoparticles but generally small amounts of sample. Volumetric procedures allow larger amounts of sample to be obtained, although nanoparticles appear mostly agglomerated. Therefore, in these methods, the synthesis of nanoparticles is not the main problem, but their manipulation is, in order to avoid the presence of large aggregates. The aim of the present work is to study the factors that affect the particle size of dense ceramic nanocrystalline composites prepared by a conventional chemical route, as in the thermal decomposition of metallic salts. In this process, the control of both grain size and agglomeration of nanoparticles is mandatory. We have found that the mean metal particle size is influenced by the anion size of the precursor salts, as also shown in other systems.<sup>13</sup> Indeed, the nucleation process of nanoparticles on ceramic particle surfaces can prevent the growth of the particles and, therefore, the nanocomposite properties can be improved. Besides, this simple method allows large amounts of sample to be obtained.

L. Klein—contributing editor

Manuscript No. 20198. Received November 5, 2003; approved July 15, 2005. Supported by the Spanish Ministry of Education and Science, under Project Number MAT 2003-04199-C02.

<sup>\*\*</sup>Fellow, American Ceramic Society.

<sup>†</sup>Author to whom correspondence should be addressed. e-mail: jsmoya@icmm.csic.es

The choice of the system ZrO<sub>2</sub>/Ni is not arbitrary. In fact, the thermal expansion coefficients of zirconia and nickel are nearly identical so that the composites do not generate thermal stresses. Zirconia ceramics are materials with fundamental properties responsible for the development of both functional and structural ceramics of interest for engineers and designers. In addition, in spite of the wide field of applications of zirconia ceramics in its pure form, conductive particles incorporated into such an insulating matrix yield new materials with appealing properties.

In previous works, different yttria-stabilized tetragonal zirconia polycrystals (Y-TZP)/nickel composites were prepared following a wet processing pressureless sintering route, with Ni particle size in the micrometer range. A wide range of metal volume fractions were studied<sup>14,15</sup> (10–40 vol%). These samples had a large fraction of porosity (5–15 vol%). There are methods to reduce this porosity, such as hot-press sintering.<sup>16</sup> However, this occurs at the cost of a large increase in nickel particle size because of the superplastic character of Y-TZP at the sintering temperatures. In this context, in the present work, we propose an alternative route to obtain dense zirconia/Ni nanocomposites by a conventional route starting from Ni salt precursors.

## II. Experimental Procedure

### (1) Starting Materials

The following commercially available salts have been used as nickel source materials: nickel (II) nitrate hexahydrate (Merck, Germany, 99.0% purity, Ni(NO<sub>3</sub>)<sub>2</sub>·6H<sub>2</sub>O), nickel (II) acetate tetrahydrate (Fluka, Switzerland, 99.0% purity, Ni(CH<sub>3</sub>COO)<sub>2</sub>·4H<sub>2</sub>O), and nickel (II) chloride hexahydrate (Merck, 98.0% purity, NiCl<sub>2</sub>·6H<sub>2</sub>O). The ceramic powders are tetragonal zirconia polycrystals (3Y-TZP; 3 mol% Y<sub>2</sub>O<sub>3</sub>; TZ-3YS, Tosoh Corp.), with an average particle size of  $d_{50} = 0.26 \mu\text{m}$ .

### (2) Nanopowder Fabrication

Nickel salt powders were weighed in order to fabricate 10 vol% Ni composites. This metal volume fraction was selected because it is high enough to detect spurious phases by X-ray diffraction (XRD) but small enough to avoid metal coalescence.<sup>17</sup> This powder was initially dissolved in alcohol by ultrasonic agitation. Subsequently, 3Y-TZP powder was mixed with the above-mentioned solution and ball milled for 24 h with ZrO<sub>2</sub> balls in alcohol media. Depending upon the salt, a suitable amount of alcohol was added to ensure the total dilution of the Ni salt. The concentrations in ethanol of the nitrate, acetate, and chloride salts were 0.96, 0.96, and 0.85 mol/L, respectively. The mixture was dried at 200°C and then calcined at 600°C for 2 h in air to obtain ZrO<sub>2</sub>/NiO mixed powders. Subsequently, the soft agglomerates in the calcined powders were crushed by wet ball milling<sup>18</sup> for 24 h. The resulting powder was dried and sieved through a 100  $\mu\text{m}$  sieve. Finally, the nickel oxide previously obtained was reduced to metallic Ni in a 90%Ar/10%H<sub>2</sub> atmosphere at 500°C for 2 h to yield a ZrO<sub>2</sub>/Ni powder.

### (3) Nickel Particle Size Distribution

XRD analysis was performed for phase identification (Philips PW 1710) and for Ni crystallite size determination (Philips X'Pert) based on the (111) peak ( $28.223^\circ$ ) linewidth. The average grain size of Ni was roughly estimated from X-ray line broadening according to Scherrer's equation,  $d = 0.9\lambda/\beta \cos \theta$ , where  $\lambda$  is the wavelength of the incident X-ray radiation (CuK $\alpha$ 1,  $\lambda = 0.15405981$  nm) and  $\theta$  is the scattering angle. The corrected peak half-width,  $\beta$ , was obtained according to the Warren formula ( $\beta^2 = B_m^2 - B_s^2$ ), where  $B_m$  is the measured peak width and  $B_s$  is the instrumental width.<sup>19,20</sup>

The Ni particle size distribution in the specimens was measured using transmission electron microscopy (TEM) images (JEOL microscope model FXII, JEM 2000 operating at 200 kV attached to a spectrometer AN 10000 Link with an Si-Li detector for microanalysis) for powdered samples, and a JEOL ARM microscope operating at 1250 keV for sintered samples. The thermal decomposition of samples was measured by differential thermal analysis (DTA) and thermogravimetric analysis (TGA, Stanton, STA 781).

### (4) Adsorption of Nickel Salts on Zirconia Surface

In order to study the adsorption of nickel salts on the surface of zirconia, two different suspensions with the same weight percent of solid content were prepared. First of all, Ni salts were dissolved in ethanol and mixed with 3Y-TZP powder. Secondly, pure 3Y-TZP powder was mixed with the corresponding diluted acid (nitric, acetic, and hydrochloric acid, respectively) in the same Ni concentration as for the salts. After 24 h stirring, the mixtures were filtered, washed four times with alcohol, and subsequently dried. Self-supporting pellets were prepared by pressing the samples diluted in KBr, and then recorded by an infrared (IR) spectrophotometer (Bruker IF66 v/s). These analyses were compared with the one corresponding to the Ni salt and the one corresponding to zirconia. X-ray photoelectron spectra (XPS) were determined for the powders obtained from the suspensions prepared with the salts. XPS spectra were recorded with a VG ESCALAB 200R system equipped with a hemispherical electron analyzer and an MgK $\alpha$ , 120 W, X-ray source. Atomic ratios were estimated by calculating the integral of each peak (or a set of them) after subtraction of an "S-shaped" (Shirley) background and using standard relative sensitivity factors.<sup>21</sup> Binding energy (BE) values were referenced to the C(1s) line at 284.6 eV (estimated accuracy =  $\pm 0.1$  eV). The magnetic hysteresis loops were measured by a vibrant sample magnetometer (ML-VSM9) with a low- and high-temperature chamber.

### (5) Sintering and Characterization

Nickel micrometer particle size 3Y-TZP/Ni (10 vol% Ni) composites, obtained by a wet-processing route, were used for a sake of comparison with nanometer nickel composites. Both micro- and nanometer-size composites conformed following the same procedure: dried powders were isostatically pressed at 200 MPa; the resulting cylindrical rods with 5 mm diameter were fired using a tubular furnace on a 90%Ar/10%H<sub>2</sub> atmosphere in two steps: (i) at 500°C for 2 h in order to reduce the NiO present in the surface of the Ni particles and (ii) at 1430°C for 2 h for final sintering. The heating and cooling rate were maintained at 60°C/h. The bulk densities of the sintered compacts were determined by the Archimedes method. The microstructures of fired specimens were examined using optical microscopy after polishing the surfaces with a 1  $\mu$ m diamond paste. Thin foils for TEM observations were obtained following a standard procedure for grinding (GATAN 656) and ion thinning (Bal-Tec, Balzers, model RES-010, 5 kV Ar<sup>+</sup> ions, incident angle 10°). Cermets were characterized by TEM using an electron microscope JEOL 2010 F (200 kV).

## III. Results

### (1) DTA-TGA

DTA and TGA curves of Ni salts precipitated on ZrO<sub>2</sub> grains were studied to determine the appropriate calcination temperature (Fig. 1). In all cases, thermal decomposition developed two stages, dehydration and decomposition, to produce NiO. In the case of Ni nitrate (Fig. 1(A)), dehydration took place from 100° to 200°C, and a clearly defined endothermic peak corresponding to the thermal decomposition of the salts into NiO was observed at around 330°C. The thermal evolution of Ni acetate salt (Fig. 1(B)) only shows two main features: the dehydration process ( $\sim 100^\circ\text{C}$ ) and the acetate decomposition to NiO ( $\sim 333^\circ\text{C}$ ). Finally, in Ni chloride (Fig. 1(C)), dehydration occurred between 100° and 200°C. An endothermic peak indicating the thermal decomposition of the salt appeared at  $\sim 672^\circ\text{C}$ .

As a compromise between the results of DTA and TGA curves, and the sintering process of zirconia and NiO, the calcination temperature of the three Ni salts on ZrO<sub>2</sub> in air was chosen to be 600°C. It should be noted that according to DTA/TGA data, the Ni chloride will not totally decompose at such temperature. However, the duration of time for the decomposition (2 h) to occur ensured that no trace of NiCl<sub>2</sub> remained in the powder. This fact was proved with the XRD patterns shown (Fig. 2). After calcination in air at 600°C for 2 h, only peaks corresponding to tetragonal zirconia, monoclinic zirconia, and nickel oxide were found by XRD in all samples (Fig. 2(A)).

### (2) XRD and TEM

The XRD technique was used to determine the Ni particle size as well. In the case of powders reduced, obtained from the

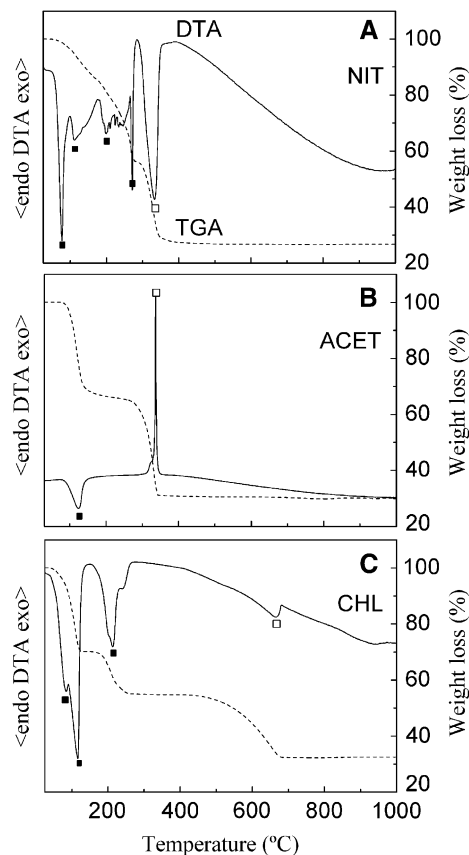


**Fig. 1.** Differential thermal analysis (DTA) (solid line) and thermogravimetric analysis (TGA) (dash line) curves for tetragonal zirconia polycrystals (3Y-TZP) powder milled in alcohol media with (A) nickel (II) nitrate hexahydrate, (B) nickel (II) acetate tetrahydrate, and (C) nickel (II) chloride hexahydrate, and then dried. Dehydration temperatures (■) and thermal decomposition (□) are indicated in the figure.

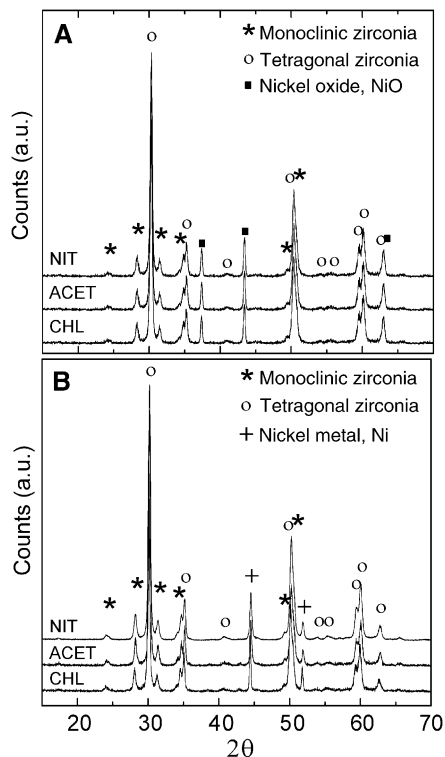


**Fig. 2.** X-ray diffraction profiles of (A) tetragonal zirconia polycrystals (3Y-TZP)/NiO powder obtained after calcination and (B) 3Y-TZP/Ni powder obtained after calcination and subsequent reduction. Sample powders were obtained from nickel (II) nitrate hexahydrate (NIT), nickel (II) acetate tetrahydrate (ACET), and nickel (II) chloride hexahydrate (CHL).

nickel chloride salt (Fig. 2(B)), the Ni(111) peak was sharp, corresponding to large particles (around 1  $\mu\text{m}$ ). The same peak was broader in the case of samples prepared from acetate ( $\sim 60$  nm) or nitrate ( $\sim 50$  nm) as the precursor and, therefore, nickel particles had a smaller size.

TEM micrographs (Fig. 3(A)) and local microanalysis on selected particles revealed that metal nanoparticles obtained from nitrate appeared homogeneous and well dispersed on the zirconia surface, and the Ni average particle size was  $\leq 50$  nm. As can be observed in Fig. 3(B), the Ni nanoparticles obtained from acetate have a heterogeneous size distribution. Mainly two particle sizes have been observed: on the one hand, particles with a size much lower than 50 nm and, on the other, particles in the 80–150 nm range.

Conversely, the sample obtained from chloride exhibited the largest Ni particle size even larger than that of the ceramic matrix particles ( $\sim 200$  nm). It should be noted that these results have been inferred not only from the analysis of the TEM micrograph (Fig. 3(C)), but also from the results of microanalysis on large selected particles (data not shown). Thus, it can be concluded that although Ni particles seem to be agglomerated because of growth during the drying or calcination processes it is difficult to determine a reliable data size distribution only by using TEM results.

### (3) Magnetic Measurements

Figure 4 shows the magnetic hysteresis loop for 3Y-TZP/10 vol% Ni powders using nitrate and chloride as the starting materials, which have the smallest Ni size and a good homogeneous dispersion of the Ni particles on the surface of the 3Y-TZP grains. The magnetization curves were obtained for applied magnetic fields ranging over  $\pm 200$  kA/m. Two sets of measurements were made at two different temperatures (90 and 300 K, respectively). The coercive force for samples obtained from nitrate salts was found to be  $H_c = 25$  kA/m at a temperature of

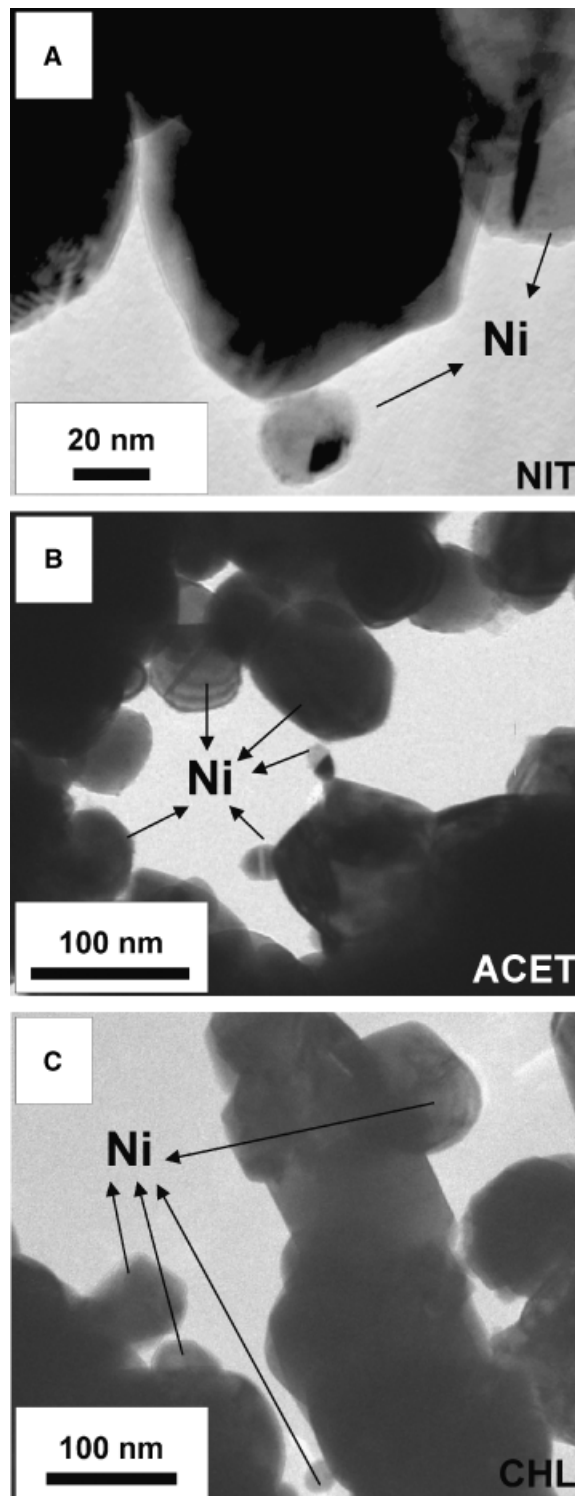


**Fig. 3.** (A) Transmission electron microscopy (TEM) image showing tetragonal zirconia polycrystals (3Y-TZP)/Ni, 10 vol%, obtained from nitrate Ni salt. (B) and (C) TEM images of samples with the same composition obtained from acetate and chloride, respectively.

90 K and  $H_c = 15$  kA/m at 300 K. However, Ni powders obtained from chloride salts presented narrower hysteresis loops at the same temperatures ( $H_c = 0.4$  and 1.1 kA/m for 90 and 300 K, respectively). As expected, the coercive force decreased as the temperature increased. The saturation magnetization was 510 kA/m at a temperature of 90 K, and 480 kA/m at 300 K for all Ni samples. These results are in good agreement with the tabulated value of Ni saturation magnetization (520 kA/m at a temperature of 90 K and 490 kA/m at 300 K).

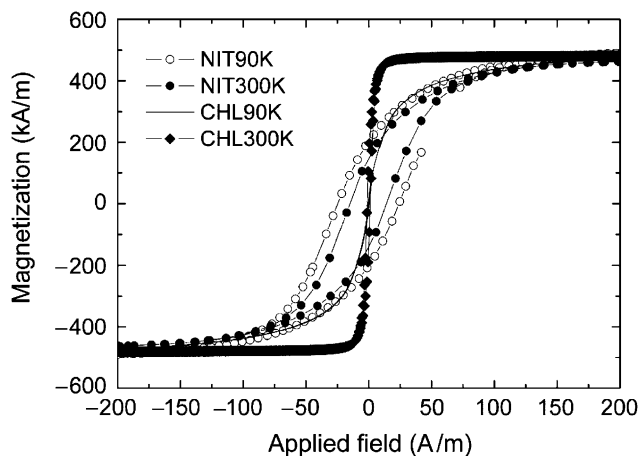


Fig. 4. Hysteresis loop corresponding to tetragonal zirconia polycrystals (3Y-TZP)/Ni 10 vol% obtained from nickel nitrate and nickel chloride measured at different temperatures (90 and 300 K).

#### (4) Infrared Spectroscopy and XPS

Infrared absorption spectroscopy (Fig. 5) and XPS (Fig. 6) have been used to elucidate the nature of the interaction of Ni salts with the powdered  $ZrO_2$  substrate. In order to investigate the degree of physisorption of each type of anion, and for comparison purposes, we have recorded the IR spectra of the three Ni salts, as well as those of the starting zirconia powder, and zirconia powder mixed with the corresponding acid (nitric, acetic, and hydrochloric, respectively).

There is a peak located at  $1384\text{ cm}^{-1}$  in the commercial zirconia sample (Figs. 5(A)–(C), curve (2)). This peak corresponds to weakly adsorbed  $NO_3^-$  species. The origin might be found in the preparation method of stabilized zirconia powders starting from  $Y(NO_3)_3$ . The  $ZrO_2$  powder stirred with nickel nitrate in alcohol media, and subsequently filtered and washed (Fig. 5(A), curve (4)) presented this band, stronger than that observed in the zirconia original powder.<sup>22</sup> The same band was found in the case of using nitric acid (Fig. 5(A), curve (3)), although weaker than that of nickel nitrate. It is noteworthy that this peak is weaker in the case of the zirconia substrate once treated with acetic acid and nickel acetate (Fig. 5(B), curves (3) and (4), respectively), and it disappears from the zirconia treated with hydrochloric acid and nickel chloride (Fig. 5(C), curves (3) and (4), respectively).

In the case of acetate, there is no experimental evidence of any adsorption of  $(COO^-)$  groups on the zirconia surface (Fig. 5(B), curve (4)), probably because of the presence of zirconia additives that hide the weak bands of acetate. In the case of nickel chloride, no impurity bands were detected (Fig. 5(C), curve (4)), but probably because the possible vibrations corresponding to modes of  $ZrCl_4$  fall in the same spectral area as those of the zirconia.

In order to gain more information about the presence of the Ni salts on the zirconia surface, Ni-containing samples prepared in the same way as for the IR spectroscopy measurements (i.e., the same solids as in Fig. 5, curve (4)) were examined with XPS. Ni was detected in all of the spectra (Fig. 6). First of all, the position of the main  $Ni(2p_{3/2})$  peak was found to be at values of BE of 855.8, 855.2, and 855.4 eV for the specimens prepared from nitrate, acetate, and chloride salts, respectively. Moreover, the presence of a strong satellite at about 6 eV higher clearly agrees with a basically Ni (II) redox state in all cases. The intensities of the Ni features varied among the samples, corresponding to Ni/Zr atomic ratios, averaged within the explored depth (ca. 2–3 nm) of 0.15, 0.04, and 0.035 for samples obtained from nitrate, acetate, and chloride, respectively. These values were calculated from the  $2p_{3/2}$  components only, as in the latter two samples the satellite of the  $Ni(2p_{1/2})$  peak was weak and could not be quantified.

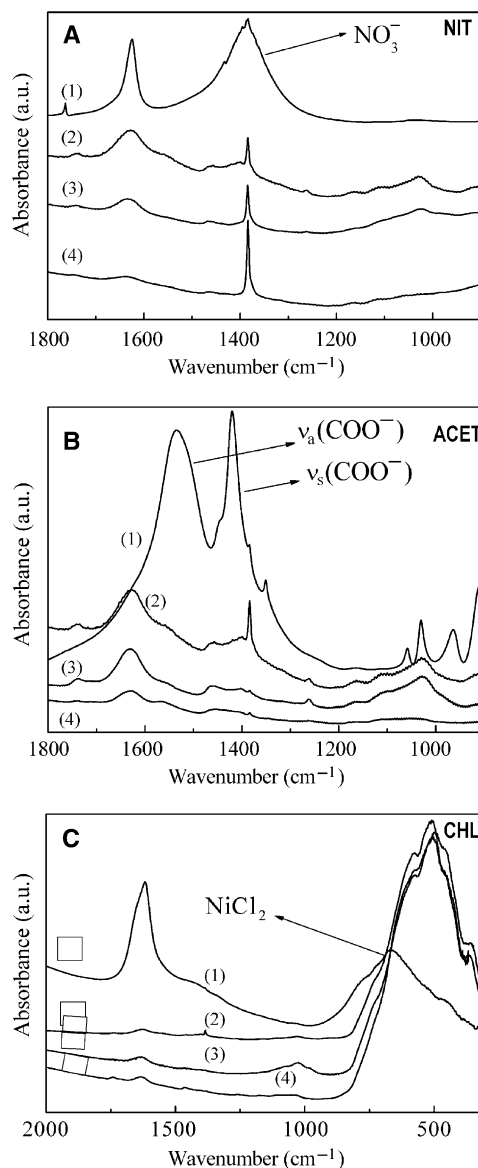
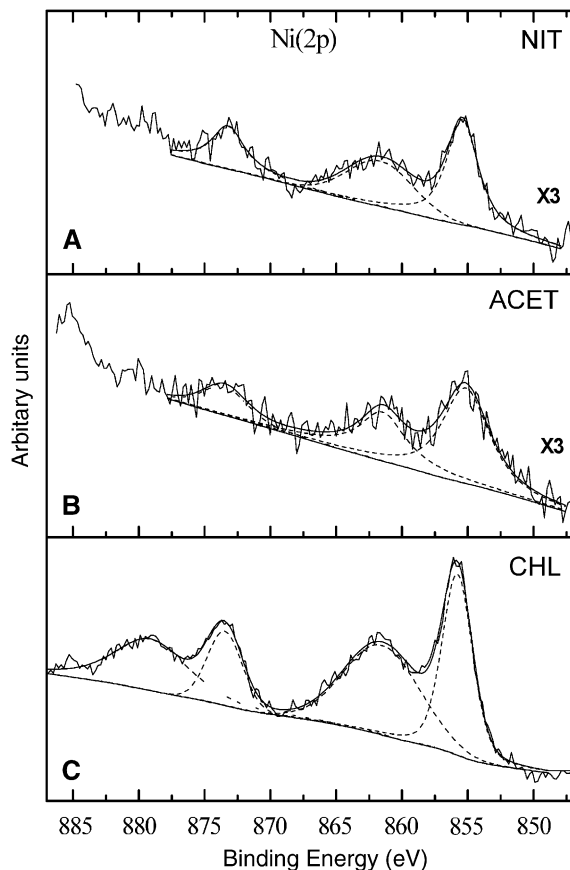


Fig. 5. Study of anion adsorption on tetragonal zirconia polycrystals (3Y-TZP) particles by infrared spectroscopy for different Ni salts: (A)  $Ni(NO_3)_2 \cdot 6H_2O$ , (B)  $Ni(C_2H_3O_2)_2 \cdot 4H_2O$ , and (C)  $NiCl_2 \cdot 6H_2O$ . (1) Ni corresponding salt, (2) as-received zirconia powders, (3) dried and washed suspension of zirconia in ethanol/acid, and (4) dried and washed suspension of zirconia in ethanol/salt. Corresponding acids are (A)  $HNO_3$ , (B)  $HC_2H_3O_2$ , and (C)  $HCl$ . Curves (2)–(4) share the same scale, but they have been shifted vertically for convenience.

Observation of the  $N(1s)$  feature was expected in the range just above  $BE = 400.0\text{ eV}$ . However, it was impeded by its relatively low sensitivity and its overlap with the Ni Auger peak occurring in these spectra in a position close to  $BE = 407.0\text{ eV}$ . Some diffuse shoulders (not shown) were observed around  $BE = 405.5\text{ eV}$ , a position that corresponds to nitrate-type species, but the mentioned overlap did not allow to ensure a relationship between them and nitrogen species, especially as the shoulder was more intense in the sample obtained from nickel acetate salt, in which, as previously mentioned, the Ni contribution was stronger. Thus, from the intensity of this shoulder, an upper limit corresponding to an atomic ratio (averaged within the explored depth) of  $N/Zr = 0.05$  could be set for the sample obtained from nickel acetate, and approximately half of that for the other two. Certainly, the value for the sample obtained from nickel nitrate did not show any higher intensity with respect to the other samples.

On the other hand, the Zr and O contributions (not shown) were as expected for zirconia. It is worth mentioning that an



**Fig. 6.** X-ray photoelectron spectra (XPS) spectra in the Ni(2p) range, obtained from tetragonal zirconia polycrystals (3Y-TZP)/Ni samples prepared from (A) Ni (II) nitrate, (B) acetate, and (C) chloride salts after washing. Note the three times higher magnification of curves (A) and (B).

important contribution from Cl (not shown) appeared in all spectra. From the intensity of the Cl(2p) peak at BE  $\approx$  195.5 eV, atomic ratios (averaged within the explored depth) Cl/Zr = 0.59, 0.65, and 0.56 were measured for these specimens. It was also noted that the intensity of the “adventitious carbon” (hydrocarbon-like contamination adsorbed from air after sample preparation) was significantly lower for the specimen obtained from nickel acetate (ratio C/Zr = 0.47) than for the other two (C/Zr = 0.76 in both), suggesting a lower tendency of organic matter adsorption in the former case (Fig. 7).

#### (5) Sintered Samples

Figure 8 shows optical micrographs of the cross-sectional microstructure of composites with 10 vol% Ni obtained from nickel nitrate, acetate, and chloride, respectively. The darker phase corresponds to zirconia and the light phase corresponds to nickel. At the magnification used, the Ni particles are difficult to distinguish in the sample obtained from nitrate. This is not the case for the sample corresponding to nickel chloride, where the metal particle size can reach values as high as 12  $\mu\text{m}$ . The sample obtained from acetate remains in an intermediate position (<5  $\mu\text{m}$ ).

The density of the sintered 3Y-TZP/Ni composites was found to be 93%–98% theoretical. The procedure presented in this work has allowed us to obtain dense nanocrystalline ceramic composites obtained from nitrate salts (Fig. 9(A)). However, in former works, this group has obtained different zirconia/nickel monolithic samples via a wet processing route by mixing nickel metal powder (Ni average particle size of 1.6  $\mu\text{m}$ ) and zirconia powder directly within a wide range of metal volume fractions. The final density of such composites after sintering ranged from 85% to 95% with regard to the theoretical value. Generally, the

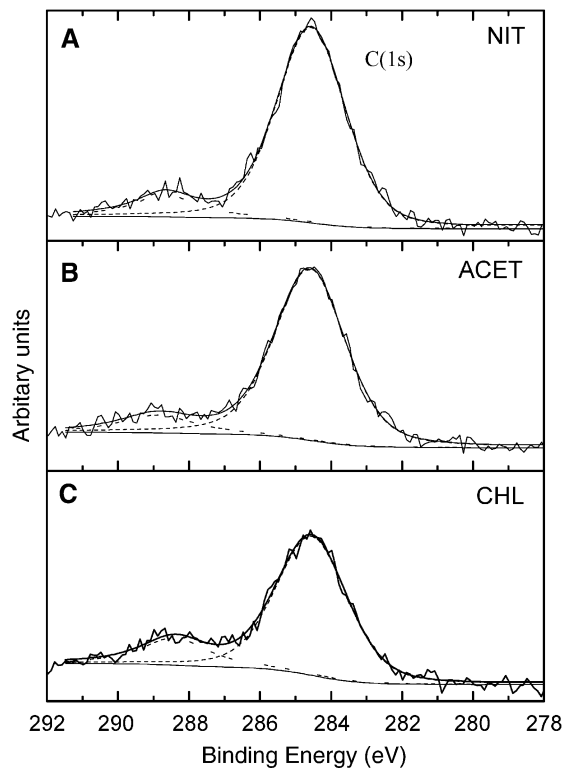


**Fig. 7.** X-ray photoelectron spectra (XPS) spectra in the C(1s) range, obtained for tetragonal zirconia polycrystals (3Y-TZP)/Ni samples prepared from Ni (II) (A) nitrate, (B) acetate, and (C) chloride salts after washing.

porosity was located around the micrometer-sized metal particles (Fig. 9(B)).

#### IV. Discussion

The study of powder TEM micrographs reveals that nickel particles obtained from nitrate present a homogeneous distribution. The Ni particle size in these samples is the smallest one compared with samples obtained from acetate and chloride salts. However, in the case of samples prepared from acetate as a precursor, nickel nanoparticles that precipitated on the zirconia surface coexist with large nickel clusters. In the case of the powders obtained from a chloride salt, the nickel particles are, at least, as large as those of the zirconia matrix.

Magnetic hysteresis loops were recorded in order to confirm whether the average nickel particle size in samples obtained from nitrate salts is in the nanometer range, as well as their dispersion within the matrix. When the particle size of a magnetic material decreases, its magnetic structure varies from a multidomain to a single-domain state.<sup>23</sup> The particle size for which nickel remains in the single-domain state ranges from 3 to 50 nm.<sup>24</sup> The magnetic properties, determined through hysteresis loops of single-domain particles, are different from those of multidomain particles in the sense that the coercive force increases notably for lower particle sizes. Moreover, the presence of large aggregates in a set of nanometer-size particles will also narrow the hysteresis loop. As a consequence, magnetic measurements can determine the particle size of a powdered sample in the nanometric scale. Under these conditions, the sample obtained from nickel nitrate exhibits a hysteresis loop with a coercive force of the order of 25 kA/m at a temperature of 90 K, and 15 kA/m at 300 K. Because large polycrystalline particles will narrow the hysteresis loop completely, we can conclude that this sample does not have large agglomerates. Therefore, all nanoparticles are well dispersed in the zirconia matrix.

No direct conclusion can be obtained about the adsorption of Ni salt anions on the zirconia surface from XPS data, because of

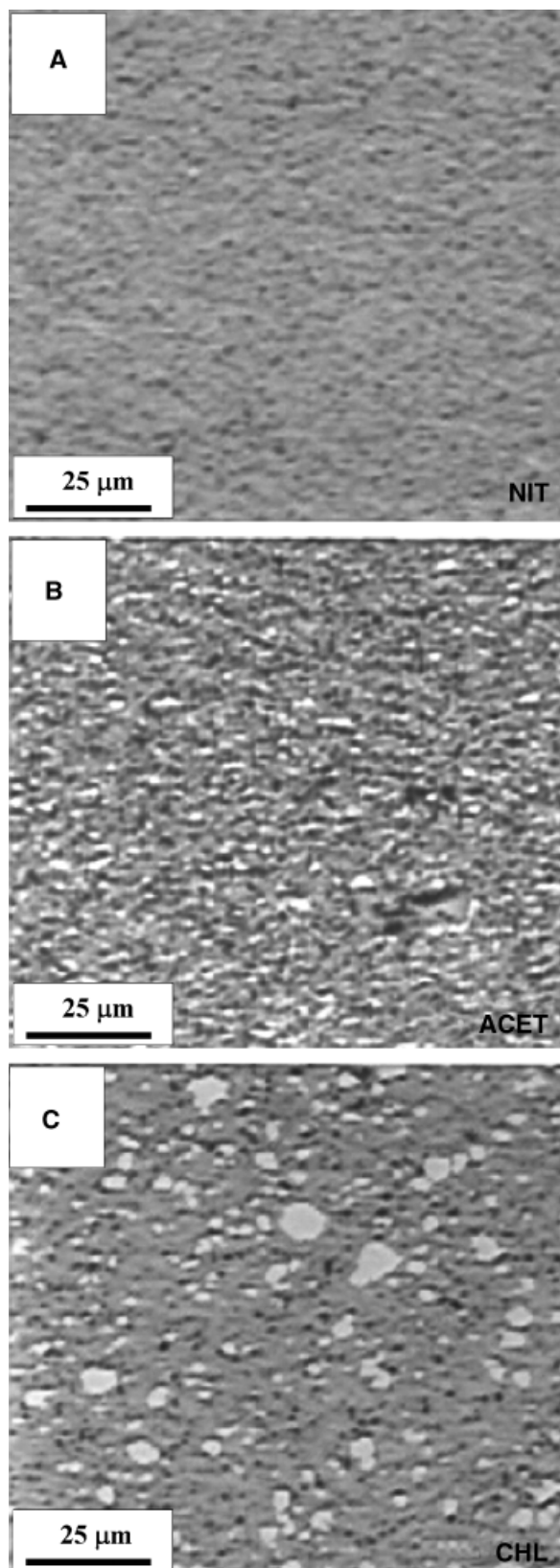


**Fig. 8.** Optical micrographs corresponding to polished cross-sections of tetragonal zirconia polycrystals (3Y-TZP)/10 vol% Ni-sintered samples obtained from (A) Ni (II) nitrate, (B) Ni (II) acetate, and (C) Ni (II) chloride.

contamination problems (in the case of Cl and C) or overlapping with other bands (N). In this case, IR spectroscopy should help to detect the presence of the  $\text{NO}_3^-$  ion weakly adsorbed on the surface of zirconia grains.<sup>23</sup> Unfortunately, such a band is

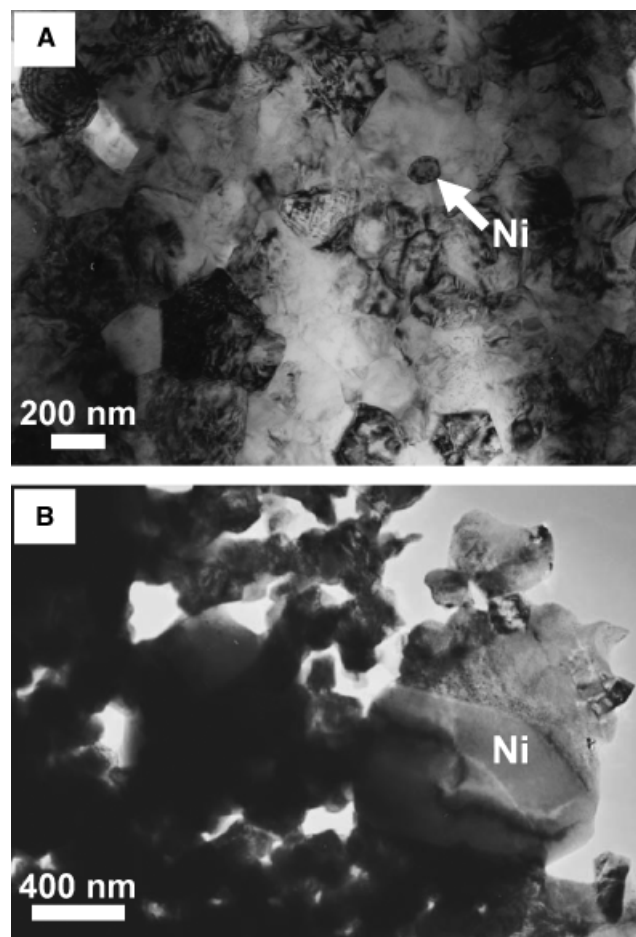


**Fig. 9.** (A) Transmission electron microscopy (TEM) image showing nanosized Ni particles in a dense sample obtained from Ni nitrate salt following the method presented in this work. (B) TEM image of sample prepared following a wet processing pressureless sintering route, where micrometer-sized Ni particles and an extremely high porosity are evident.

present for all three samples (Figs. 5(A)–(C), curve (2)), because of its presence in the initial zirconia material, and again a direct conclusion is not possible. However, a quantitative analysis of the  $1384\text{ cm}^{-1}$  peak reveals that it disappears from the zirconia substrate once treated with an acid solution of some other anion, such as  $\text{Cl}^-$  (Fig. 5(C), curve (3)). On the contrary, this peak notably increases in the case of the zirconia powder treated with Ni nitrate salt (Fig. 5(A), curve (4)), being even larger than that of the powder treated with  $\text{HNO}_3$  (Fig. 5(A), curve (3)). This suggests that the whole molecule of the nickel nitrate is adsorbed on the zirconia surface.

However, markedly different Ni/Zr ratios were detected by XPS in the three types of washed precursor samples, even though the volume fraction of nickel was the same for each sample. It was found to be the lowest in the sample obtained for the nickel nitrate case, and especially high in that obtained from the nickel acetate salt. This latter observation suggests that, in the presence of acetate, the adsorption properties of zirconia (which probably controls the amount of Ni retained after washing) have changed. Such an indication may be coupled with the observation that the amount of XPS-detected surface carbonaceous species is lowest in the case of acetate, in spite of the fact that an organic anion is used. A lower tendency to adsorb organic impurities from the ambient atmosphere suggests a less acidic character of the surface; this agrees with the more basic character of acetate anion in comparison with nitrate or chloride. Thus, it could be postulated that, in this case, the zirconia surface may be more populated by basic  $\text{OH}^-$  groups, which could lead to a higher amount of adsorbed  $\text{Ni}^{2+}$  cations during

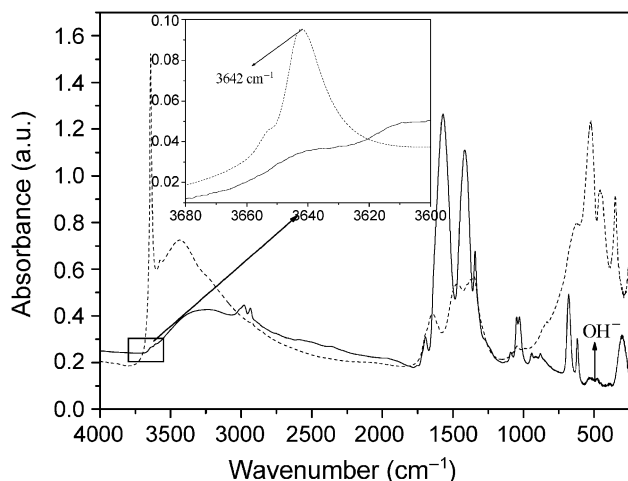


**Fig. 10.** Infrared spectra of nickel (II) nitrate on zirconia surface (continuous line).  $\text{Ni}(\text{OH})_2$  infrared spectra drawn for reference (dashed line). Inset: details of the band owing to the presence of  $\text{Ni}(\text{OH})_2$ .

preparation. This might contribute to the presence of a fraction of highly dispersed Ni (within a very heterogeneous size distribution, as detected by TEM) in that obtained from the nickel acetate salt sample. Taking into account the possible effects of the basic character of the acetate by these XPS data, one may think that  $\text{Ni}(\text{OH})_2$  might be formed, together with  $\text{Ni}(\text{CH}_3\text{COO})_2$ , during the preparation of the material. The presence of  $\text{Ni}(\text{OH})_2$  has been demonstrated by the  $3645\text{ cm}^{-1}$  mode assigned to  $\text{Ni}(\text{OH})_2$  (Fig. 10). This might also provide an explanation for the heterogeneous size distribution in samples obtained from acetate salts. Since the  $\text{OH}^-$  ion has a smaller size than  $\text{CH}_3\text{COO}^-$  ion, the electrostatic Madelung stabilization energy of  $\text{Ni}(\text{OH})_2$  will be higher than that of  $\text{Ni}(\text{CH}_3\text{COO})_2$ . Thus, Ni particles obtained from  $\text{Ni}(\text{OH})_2$  have a higher particle size than those obtained from  $\text{Ni}(\text{CH}_3\text{COO})_2$ , giving rise to a heterogeneous particle size distribution.

Using the same reasoning, the large  $\text{NO}_3^-$  anion would lead to deposited salt crystals smaller than the  $\text{Cl}^-$  or  $\text{OH}^-$  anions. Thus, the lower Ni particle size obtained using nitrate salt can be justified.

These results can be confirmed in the sintered samples, as can be observed in Fig. 8. We could only obtain agglomerate-free nanostructured composites in the case of starting from nanometric Ni particles. The best results were obtained from powders using a nitrate solution as a precursor. Moreover, this kind of composites presented porosity values lower than 2 vol% even though they were sintered by a conventional pressureless route.

## V. Conclusions

In the present work, the processing of 3Y-TZP/10 vol% Ni nanopowders via calcination and subsequent reduction from three different Ni salts (Ni (II) nitrate, chloride, and acetate) to obtain nanodispersed Ni particles has been established. It has been found that the size of the anion is probably the factor that mostly determines the final Ni particle size. The smallest anions lead to the formation of larger crystals during preparation, which influence the size of the final product. This is the case for Ni particles obtained from chloride salt, which have a small precursor anion, and the resultant Ni particle size is larger than in the other two cases. The Ni particles obtained from nitrate are the smallest ones, and they are better dispersed in the matrix.

Magnetic measurements of samples obtained from nitrate indicate a magnetic single-domain structure. Thus, only in the case where single nanoparticles appear perfectly dispersed and attached to the zirconia particles will it be possible to obtain truly zirconia-Ni nanocomposites, with Ni particle size around 50 nm. In the case of using acetate as a precursor, the Ni particles

present a heterogeneous distribution. This result has been explained through the formation of  $\text{Ni}(\text{OH})_2$  in the suspension, which is a consequence of the lowest acidity. Finally, the results obtained in the present work indicate that the main factors that allow Ni nanoparticles to precipitate on a ceramic matrix are the following: the metallic precursor may be a salt only if its anion is a large one and if the metallic cations remain in solution without reacting with other chemical species.

## Acknowledgments

Thanks are due to E. Pardo for assistance in recording the XPS spectra, as well as to L. Gremillard for his help with the observation of the samples by TEM.

## References

- H. Hwang, K. Tajima, M. Sando, and M. Toriyama, "Fatigue Behavior of PZT-Based Nanocomposites with Fine Platinum Particles," *J. Am. Ceram. Soc.*, **81** [12] 3325–8 (1998).
- M. Lieberthal and W. Kaplan, "Processing and Properties of  $\text{Al}_2\text{O}_3$  Nanocomposites Reinforced with Sub-Micron Ni and  $\text{NiAl}_2\text{O}_4$ ," *Mater. Sci. Eng. A*, **302**, 82–91 (2001).
- S. Oh, T. Sekino, and K. Niihara, "Fabrication and Mechanical Properties of 5 vol% Copper Dispersed Alumina Nanocomposite," *J. Eur. Ceram. Soc.*, **18**, 31–7 (1998).
- H. Hyuga, Y. Hayashi, T. Sekino, and K. Niihara, "Fabrication Process and Electrical Properties of  $\text{BaTiO}_3/\text{Ni}$  Nanocomposites," *Nanostruct. Mater.*, **9**, 547–50 (1997).
- J. S. Helman and B. Abeles, "Tunneling of Spin-Polarized Electrons and Magnetoresistance in Granular Ni Films," *Phys. Rev. Lett.*, **37** [21] 1429–32 (1976).
- D. Kumar, H. Zhou, A. Kvit, and J. Narayan, "Improved Magnetic Properties of Self-Assembled Epitaxial Nickel Nanocrystallites in Thin-Film Ceramic Matrix," *J. Mater. Res.*, **17** [4] 738–42 (2002).
- M. Nawa, T. Sekino, and K. Niihara, "Fabrication and Mechanical Behavior of  $\text{Al}_2\text{O}_3/\text{Mo}$  Nanocomposites," *J. Mater. Sci.*, **29** [12] 3185–92 (1994).
- T. Sekino and K. Niihara, "Microstructural Characteristics and Mechanical Properties for  $\text{Al}_2\text{O}_3/\text{Metal}$  Nanocomposites," *Nanostruct. Mater.*, **6** [5–8] 663–6 (1995).
- K. Hiroki, S. Tohru, K. Takafumi, N. Tadachika, and K. Niihara, "Ceramic Processing Science VI"; pp. 867–72 in *Ceramic Transactions*, Vol. 12, Edited by S. -I. Hirano, G. L. Messing, and N. Claussen. The American Ceramic Society, Westerville, OH, 1993.
- CH. Laurent, A. Peigney, O. Quénard, and A. Rousset, "Synthesis and Mechanical Properties of Nanometric Metal Particles–Ceramic Matrix Nanocomposites," *Sil. Ind.*, **63** [5–6] 77–84 (1998).
- C. A. Schuh, T. G. Nieh, and T. Yamasaki, "Hall-Petch Breakdown Manifested in Abrasive Wear Resistance of Nanocrystalline Nickel," *Scripta Mater.*, **46**, 735–40 (2002).
- E. Breval, G. Dodds, and C. G. Pantano, "Properties and Microstructure of Ni–Alumina Composite Materials Prepared by the Sol/Gel Method," *Mater. Res. Bull.*, **20** [10] 1191–205 (1985).
- L. A. Diaz, A. F. Valdés, C. Díaz, A. M. Espino, and R. Torrecillas, "Alumina/Molybdenum Nanocomposites Obtained in Organic Media," *J. Eur. Ceram. Soc.*, **23**, 2829–34 (2003).
- C. Pecharrómán, S. López-Esteban, J. F. Bartolomé, and J. S. Moya, "Evidence of Nearest-Neighbor Ordering in Wet-Processed Zirconia–Nickel Composites," *J. Am. Ceram. Soc.*, **84** [10] 2439–41 (2001).
- S. López-Esteban, J. F. Bartolomé, and J. S. Moya, "Mechanical Performance of 3Y-TZP/Ni Composites: Tensile, Bending, and Uniaxial Fatigue Tests," *J. Mater. Res.*, **17** [7] 1592–600 (2002).
- H. Kondo, T. Sekino, Y.-H. Cho, T. Kusunose, T. Nakayama, M. Wada, T. Adachi, and K. Niihara, "Mechanical and Magnetic Properties of Nickel-Dispersed Tetragonal Zirconia Nanocomposites," *J. Nanosci. Nanotech.*, **2** [5] 485–90 (2002).
- C. Pecharrómán, F. Esteban-Betegón, J. F. Bartolomé, G. Richter, and J. S. Moya, "Theoretical Model of Hardening in Zirconia–Nickel Nanoparticle Composites," *Nanoleters*, **4** [4] 747–51 (2004).
- S. Oh, M. Sando, and K. Niihara, "Processing and Properties of Ni–Co Alloy Dispersed  $\text{Al}_2\text{O}_3$  Nanocomposites," *Scripta Mater.*, **39** [10] 1413–8 (1998).
- V. Srdic, M. Winterer, A. Möller, G. Miehe, and H. Hahn, "Nanocrystalline Zirconia Surface-Doped with Alumina: Chemical Vapor Synthesis, Characterization, and Properties," *J. Am. Ceram. Soc.*, **84** [12] 2771–6 (2001).
- A. R. West, *Solid State Chemistry and Its Applications*, pp. 173–5. John Wiley and Sons, Great Britain, 1987.
- C. D. Wagner, L. E. Davis, M. V. Zeller, J. A. Taylor, R. M. Raymond, and L. H. Gale, "Empirical Atomic Sensitivity Factors for Quantitative Analysis by Electron Spectroscopy for Chemical Analysis," *Surf. Interface Anal.*, **3**, 211 (1981).
- K. I. Hadjiivanov, "Identification of Neutral and Charged  $\text{N}_x\text{O}_y$  Surface Species by IR Spectroscopy," *Catal. Rev.-Sci. Eng.*, **42** [1–2] 71–144 (2000).
- C. Kittel, J. K. Galt, and W. E. Campbell, "Crucial Experiment Demonstrating Single Domain Property of Fine Ferromagnetic Powders," *Phys. Rev.*, **77**, 725 (1950).
- B. D. Cullity, *Introduction to Magnetic Materials*, pp. 117–9 and 309–11. Addison-Wesley, California, 1972. □